POTENTIAL DISTRIBUTION IN METAL-VACUUM-METAL PLANAR BARRIERS CONTAINING SPHERICAL PROTRUSIONS OR INCLUSIONS

A. Lucas, J. Vigneron, J. Bono, P. Cutler, T. Feuchtwang, R. Good, Jr. Huang, Z. Huang

JOURNAL DE PHYSIQUE
Colloque C9, supplément au n°12, Tome 45, décembre 1984

POTENTIAL DISTRIBUTION IN METAL-VACUUM-METAL PLANAR BARRIERS CONTAINING SPHERICAL PROTRUSIONS OR INCLUSIONS +

A.A. Lucas, J.P. Vigneron, J. Bono*, P.H. Cutler*, T.E. Feuchtwang*, R.H. Good, Jr* and Z. Huang*

Départment de Physique, F.N.D.P., 61, rue de Bruxelles, 5000 Namur, Belgium
**Physics Department, The Pennsylvania State University, University Park, Pennsylvania 16802, U.S.A.*

Résumé - On présente une méthode exacte pour le calcul rapide a) de la distribution de potentiel électrostatique régnant entre deux électrodes planes parallèles contenant une protrusion sphérique ou insertion sphérique conductrice et soumises à une différence de potentiel et b) du potentiel image classique ressenti par un électron traversant la jonction plano-sphérique.

Abstract - We present an exact method for the fast computation of a) the electrostatic potential distribution between two biased planar, parallel electrodes containing a spherical protrusion or an isolated conducting, spherical insertion and b) the classical image charge potential experienced by an electron crossing the plano-spherical junction.

I - INTRODUCTION

Interest in tunneling through non planar MVM junctions has recently been enhanced by the advent of the Scanning Tunneling Microscope (STM)[1].

Theoretical models[2,3,4] have been constructed aiming at a better understanding of the observed spatial resolution of the microscope.

Prior to this, theoretical work [5] had been concerned with nonplanar tunneling in metal whisker diodes which have a geometry similar to STM and which were instrumental in establishing the recently defined velocity of light[6]. Also, tunneling through curved interfaces occurs in electroluminescent MOM junctions[7] where the luminescence is enhanced by roughness.

In discussing the tunneling in STM, it may be important to use realistic models of the junctions[8]. In one such model the tip surface is a planar conductor provided with a hemispherical protrusion which models an atomic cluster through which the tunnel current is believed to pass in the actual device. The actual imperfections are not expected to have such regular shapes but this model permits a theoretical analysis and is expected to give a first approximation to actual experimental conditions. The counter electrode representing the surface to be examined by STM is here a flat metal conductor separated from the tip by a vacuum gap.

In this paper we report on methods of solving two problems :
1) Determination of the three-dimensional potential barrier due to the external bias field. That is, given the potentials at the two electrodes, determine the poten-

+ This research was supported in part by the NATO Research Grants Program, Grant no 1902, Scientific Affairs Division, Brussels, Belgium and the Office of Naval Research, Arlington, Virginia, Contract No. N00014-82-K-0702.

tial distribution in the space between them.

2) Determination of the classical image charge potential. That is, with the electrodes grounded and a point charge in the space between them, calculate the potential energy of the system as a function of the position of the point charge.

The sum of these two potential barriers represents the classical vacuum potential barrier across which the electrons in a STM tunnel.

The solution for the static potential obtained here could also be derived by solving Maxwell's equations and boundary conditions for the corresponding quasi static problem in which the metal electrodes are represented by a local, frequency-dependent dielectric function $\varepsilon(\omega)$. Such an approach, which would also give the resonant modes of the MVM junction, has recently been adopted by Ruppin[9] (who used a general method due to Berreman[10]) for a single planar electrode with one hemispherical bump, in the context of Surface Enhanced Raman Scattering.

As expected, for realistic values of the geometrical length parameters, the tunneling barrier exhibits strong deviations from the planar MVM barrier of the same materials. In particular, substantial narrowing of the barrier along the axial direction of the tip and large barrier asymmetry with respect to bias reversal are obtained. Graphical representation of these numerical results will be presented and discussed.

II - STATIC BIAS POTENTIAL DISTRIBUTION

We will treat the general case of fig. 2 which covers all situations of partially protruding spheres ($a \leqslant R$) or isolated spherical inclusions ($a > R$) such as found in roughened electroluminescent MOM junctions.

The first thing we do is to reflect in the plane z=0 both the vacuum gap and the sphere of fig. 2, as shown in fig. 3. It is easy to convince oneself that the potential distribution in the upper half ($z > 0$) of the double gap coincides, by symmetry, with the potential of the actual junction of fig. 2.

The potential at $\vec{r}$ would be known if we knew the induced surface charge density σ on all surfaces. In fact, the knowledge of the surface charge density $\sigma(\vec{r}_0)$ on the upper sphere will suffice if we observe that

i) by symmetry, the surface charge density on the lower sphere is identical to $\sigma(\vec{r}_0)$ and

ii) employing the method of images to satisfy the boundary conditions, the surface charge density on the planar conductors at d and -d can be replaced by an infinite series of spherical charge distributions obtained by imaging the two spheres in the twin mirrors at d and -d.

Thus the problem is entirely reduced to calculating the potential due to a linear array of identical spheres, clustered by pairs, and all carrying the same charge density $\sigma(\vec{r}_0)$ as the real sphere S_0. It is clear that if we obtain the potential at $\vec{r}$ due to S_0 alone, we can obtain the total potential by adding up the image sphere contributions through suitable translations of the z coordinate. Let us write the axially symmetric total potential at $\vec{r} = (\rho,z)$ as

$$V(\rho,z) = V_0 \frac{z}{d} + V'(\rho,z) \qquad (1)$$

where we have separated the simple planar gap contribution $V_0 z/d$ which must be recovered for asymptotically large ρ. The perturbation V' satisfies the boundary conditions

$$\begin{aligned} V' &= 0 \quad \text{for } z = 0 && (a) \\ V' &= 0 \quad \text{for } z = \pm d && (b) \\ V' &= -\frac{V_0}{d} z \text{ on } S_0 && (c) \end{aligned} \qquad (2)$$

Let us expand σ in Legendre polynomials :

$$\sigma(\vec{r}_o) = \sum_{\ell=1}^{\infty} A_\ell \, P_\ell(\cos\theta_o) \tag{3}$$

where the $\ell = 0$ term is excluded for charge neutrality. The potential due to the real sphere is given by

$$V_o'(\vec{r}) = R^2 \int_{S_o} d\Omega_o \frac{\sigma(\theta_o)}{|\vec{r}_a - \vec{r}_o|} \tag{4}$$

where $\vec{r}_a$ is the position of point P with respect to the center of the sphere S_o. Inserting the generating function of the P's

$$\frac{1}{|\vec{r}_a - \vec{r}_o|} = \sum_{k=o}^{\infty} \frac{R^k}{r_a^{k+1}} P_k(\cos\alpha) \tag{5}$$

and using the addition theorem of spherical harmonics

$$P_k(\cos\alpha) = \frac{4\pi}{2k+1} \sum_{m=-k}^{+k} Y_k^{m\star}(\theta_o, \phi_o) \, Y_k^m(\theta,\phi) \tag{6}$$

in (4) gives

$$V_o' = 4\pi R^2 \sum_{\ell k m} A_\ell \frac{R^k}{2k+1} \frac{1}{r_a^{k+1}} Y_k^m(\theta,\phi) \int_{S_o} d\Omega_o \, P_\ell(\cos\theta_o) \, Y_k^{m\star}(\theta_o,\phi_o) \, .$$

Orthogonality of the Y_k^m's reduces V_o' to

$$V_o' = \sum_{\ell=1}^{\infty} B_\ell \frac{1}{(\rho^2+z_a^2)^{\frac{\ell+1}{2}}} P_\ell\left(\frac{z_a}{\sqrt{\rho^2+z_a^2}}\right)$$

where $z_a = z - a$, and B_ℓ are new unknown coefficients, proportional to A_ℓ.

Now we can add contributions to the potential from all spheres centered at $z_n = \pm(a+2nd)$, $n = 1,2,\ldots$. The final result is

$$V'(\vec{r}) = \sum_{\ell=1}^{\infty} B_\ell \, F_\ell(\rho,z) \tag{8}$$

$$F_\ell(\rho,z) = \sum_{n=-\infty}^{\infty} [\rho^2 + (z-2nd-a)^2]^{-\frac{\ell+1}{2}} P_\ell\left[\frac{z-2nd-a}{\sqrt{\rho^2 + (z-2nd-a)^2}}\right]$$

$$- (-1)^\ell [\rho^2 + (z+2nd+a)^2]^{-\frac{\ell+1}{2}} P_\ell\left[\frac{z+2nd+a}{\sqrt{\rho^2 + (z+2nd+a)^2}}\right] \tag{9}$$

It is easy to verify that F_ℓ is antisymmetric (change n into -n)

$$F_\ell(\rho,-z) = - F_\ell(\rho,z) \tag{10}$$

which guarantees the boundary condition (3-a). By virtue of the image construction, F_ℓ also satisfies (the nth term cancels the -(n+1)th term) $F_\ell(\rho,+d) = 0$ which guarantees the boundary condition (3-b). Finally, the unknown coefficients B_ℓ are determined by imposing the last condition (3-c) :

$$\sum_{\ell=1}^{\infty} B_\ell \, F_\ell(\rho,z) = - \frac{V_o}{d} z \tag{11}$$

$$\text{for} \quad a-R \leqslant z \leqslant a+R, \qquad \rho^2 = R^2-z^2 \tag{12}$$

The B_ℓ coefficient for ℓ up to an upper multipolar limit L can be found as the solutions of a set of L linear equations obtained by imposing the condition (11) at L distinct values of z suitably chosen in the indicated interval. However it is more accurate to determine the first L coefficients by least square adjusting[11] them to a much larger number $N \gg L$ of equations (11) written for N distinct values of z.

For a hemispherical protrusion (a = 0), the solution (8) (9) reduces to

$$V'(\vec{r}) = \sum_{\ell=1}^{\infty} C_\ell \, F_\ell(\rho,z) \tag{13}$$

$$F_\ell(\rho,z) = \sum_{n=-\infty}^{\infty} [\rho^2 + (z+2nd)^2]^{-\ell} \, P_{2\ell-1}\left[\frac{z+2nd}{\sqrt{\rho^2 + (z+2nd)^2}}\right] \tag{14}$$

and, by symmetry, involves only odd multipoles. It turns out that the convergence of the n-summation over the images in (14) is very fast ($n \leqslant 10$ suffices to get the F_ℓ with 10^{-5} accuracy). Regarding the multipole expansion, taking $\ell \leqslant 3$ proves sufficient to determine the C_ℓ's with 10^{-5} accuracy. A few equipotentials are illustrated in fig. 4. The potential values along the axial z direction ($\rho = 0$) are plotted in fig. 5. The characteristic buldging out of the potential, as compared to the linear behaviour of a planar MVM junction, is clearly seen. It reflects the enhancement of the electric field at the sphere apex.

III - ELECTRON MULTIPLE IMAGE

The construction of the self image potential of the tunneling electron is straightforward when using an appropriate sequence of multiple images. We illustrate the principle of the method for the case of a hemispherical protrusion which, as is well known, presents the simplifying feature of requiring only three images in the non planar electrode (fig. 6).

Let us denote (q,ρ_q,z_q) the charge and position of the tunneling particle. This has exactly three images in the lower electrodes given by $(q', \rho_{q'}, z_{q'})$,$(-q',\rho_{q'},-z_{q'})$ and $(-q,\rho_q,-z_q)$ where

$$q' = - q \frac{R}{r_q} \quad \text{and} \qquad \frac{z_{q'}}{z_q} = \frac{\rho_{q'}}{\rho_q} = \frac{R^2}{r_q^2} \tag{15}$$

The source charge q and its three images in the lower electrode are considered as the first generation of an infinite set of generations constructed as shown in fig. 6. The second generation, also having 4 charges, is simply the images in the plane z = d of the previous charges. Each of the new charges in the upper electrode gives rise to exactly three new image charges in the lower electrode and so forth. Thus, the 2nth and (2n-1)th generations have the same number of charges, namely 4.3^{n-1} ($n = 1,2,\ldots,\infty$).

Once the image charge array q_i has been constructed, the self image potential energy of the source charge q is written as

$$W = +\frac{1}{2} q \sum_i \frac{q_i}{|\vec{r}-\vec{r}_i|} \tag{16}$$

where the factor 1/2 takes account of the induced nature of the images[12].

Each charge generation being neutral, the potential calculated from (16) converges very fast : 10 generations suffice to get W with an accuracy of 10^{-5}. One typical result is illustrated in fig. 7 for $\rho = 0$. The image potential energy is also slightly asymmetrical as expected and, of course, diverges at z = R and z = d. If desired, this can be easily corrected in the usual way by withdrawing the image planes slightly inside the conductors. These image potential values must be added to the static bias potential of fig. 4 to construct the tunnel barrier through the protrusion[12].

IV - CONCLUSION

The most important result of the present calculations is to demonstrate the dominant role of the classical multiple image potential in determining the shape of the vacuum barrier in the STM junction where the static bias potentials are on the order of 10 meV. Consequently, it is essential to recognize the nonseparability of this barrier which precludes the use of a one-dimensional transmission coefficient for tunneling calculations in a realistic model of the STM. A more complete discussion of the calculated barriers and the significance in three-dimensional tunneling will be published elsewhere.

REFERENCES

1. G. Binnig, H. Bohrer, Ch. Berber and E. Weibel, Phys. Rev. Letters 49, 57 (1982); Phys. Rev. Letters 50, 120 (1983).
2. J. Tersoff and D. Hamann, Phys. Rev. Lett. 50, 1998 (1983).
3. N. Garcia, C. Ocal and F. Flores, Phys. Rev. Lett. 50, 2002 (1983).
4. A. Baratoff, Europhysics Conference Abst. 7b, 364 (1983).
5. T.E. Feuchtwang, P.H. Cutler, N.M. Miskowsky and A.A. Lucas, "Quantum Metrology and Fundamental Physical Constants", ed. by P.H. Cutler and A.A. Lucas, NATO ASI Series B, vol. 98, p. 529 (1983). Plenum Press, New York.
6. K.M. Evenson, "Quantum Metrology and Fundamental Physical Constants", ed. by P.H. Cutler, N.M. Miskowsky and A.A. Lucas, NATO ASI Series B, vol. 98, p. (1983). Plenum Press, New York.
7. A. Adamson, J.C. Wyss and P.K. Hansma, Phys. Rev. Lett. 32, 545 (1978).
8. T.E. Feuchtwang, P.H. Cutler and N.M. Miskowsky, Phys. Lett. 99A, 167 (1983).
9. R. Ruppin, Solid State Comm. 39, 903 (1981).
10. D.W. Berreman, Phys. Rev. 163, 855 (1967); Phys. Rev. B1, 381 (1970).
11. G.E. Forsythe, M.A. Malcolm and C.B. Moler, Computer Methods for Mathematical Computations. Prentice-Hall, Englewood Cliffs, 1977.
12. Proper inclusion of the factor 1/2 in the image potential is important for calculating the tunnel current, as shown in N.M. Miskowsky, P.H. Cutler, T.E. Feuchtwang and A.A. Lucas, Appl. Phys. A27, 139 (1982).

Fig. 1

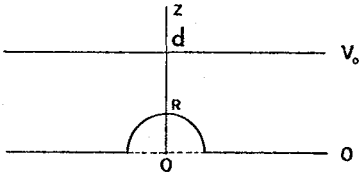

Figure 1

Model planar MVM junction with hemispherical protrusion.

Fig. 2

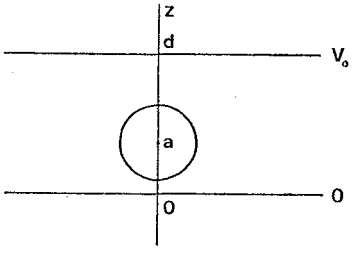

Figure 2

Model planar MVM junction with spherical inclusion.

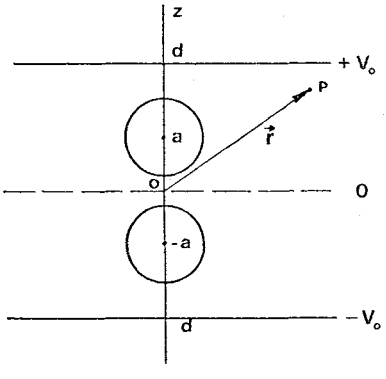

Figure 3

Antisymmetrical duplication of the junction of Fig. 2

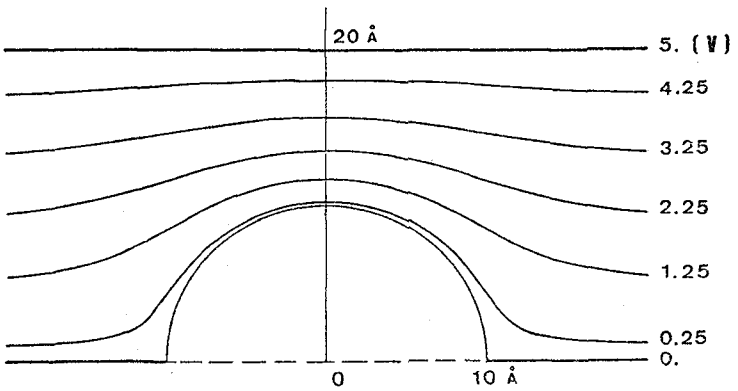

Figure 4

Equipotential lines in the MVM junction biased to 5 V.

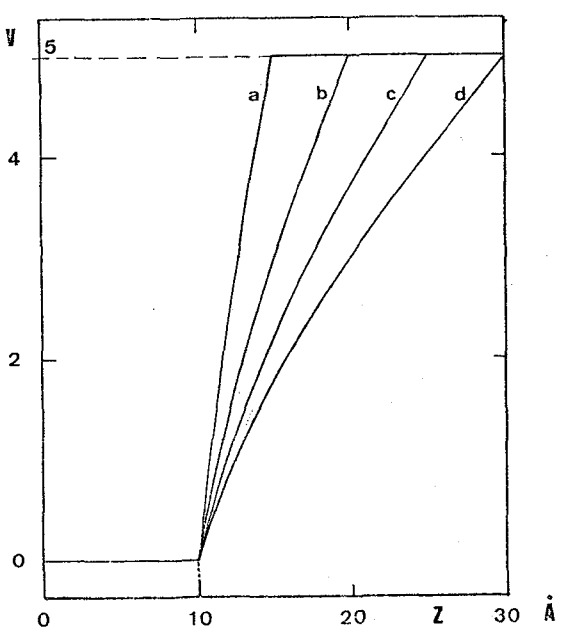

Figure 5

Potential distributions in the vacuum gap of a junction biased to 5 V. a, b, c and d correspond to a width of 5, 10, 15 and 20 Å respectively. The hemispherical protrusion has a radius of 10 Å.

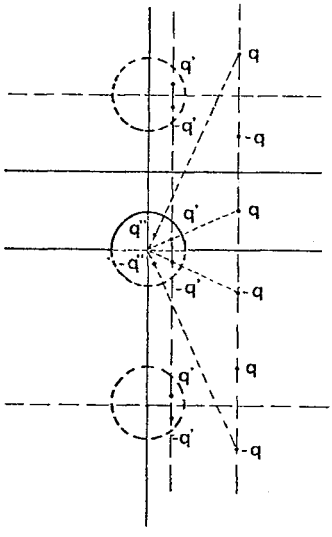

Figure 6 - Iteration method to generate the set of multiple images of the object charge q in the vacuum gap of a junction with hemispherical protrusion.

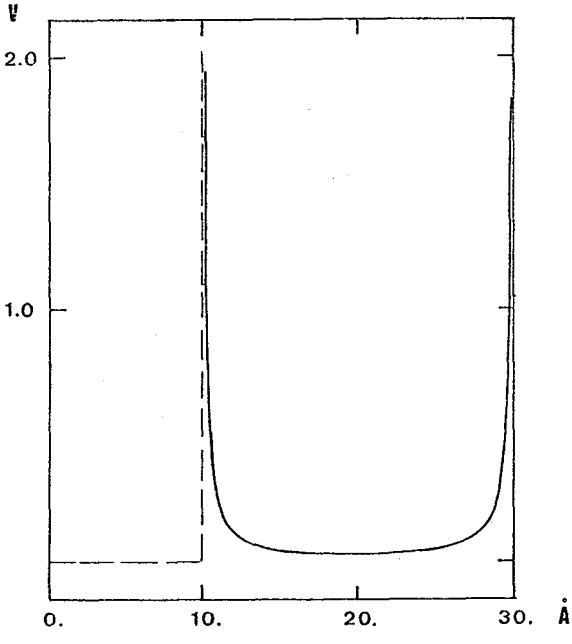

Figure 7 - Self-image potential along the symmetry axis for a charge in a junction of 30 Å width having a hemispherical protrusion of 10 Å.